New Insight into minimal architecture based carbon nanotubes anode with improved mechanical properties for Li-ion battery

Satish Teotia[1,3], B.P. Singh[1]*, Anisha Chaudhary[1], Indu Elizabeth[2], Anchal Srivastava[3], Saroj Kumari[1], S. R. Dhakate[1], S. Gopukumar[2], R. B. Mathur[1]

[1]*Advanced Carbon Products, CSIR-National Physical Laboratory, New Delhi 110012, India*
[2]*CSIR-Central Electro Chemical Research Institute, Karaikudi, Chennai 630006, India*
[3]*Department of Physics, Banaras Hindu University, Varanasi 221005, UP, India*

*Corresponding author: Tel: (+91) 11-45608460; Fax: (+91)-11-45609310;
E-mail: bps@nplindia.org, bpsingh2k4@yahoo.com

Abstract

The quick advancement of flexible energy storage gadgets has persuaded individuals to look for reliable electrodes with high mechanical flexibility and remarkable electrochemical performance. In the present study, we demonstrate a simple and scalable process to fabricate a flexible, light-weight, free-standing polyvinylidene fluoride-multiwalled carbon nanotubes (PVDF-MWCNT) composite paper, which can be specifically utilized as a flexible anode for lithium ion batteries (LIBs). The excellent binding of MWCNT with PVDF matrix, developed by a straightforward vacuum filtration process, provides sufficient structural integrity to the composite paper. The breaking strength of the PVDF-MWCNT composite paper so formed is found to be 3.5 MPa with strain to failure of 11.25%. The composite paper so developed shows a good cycle reversible charge capacity when used as anode in a standard Li-ion battery. The PVDF-MWCNT composite paper provides a novel pathway to large scale fabrication of flexible electrodes which can be used without conducting support of copper sheet. Copyright © 2017 VBRI Press.

Keywords: MWCNT, flexible, free-standing, composite, anode, Li-ion battery.

Introduction

In recent years, the interest of research community is centered on the development of the effective energy storage strategies with the prospective to replace traditional energy sources as well as fulfill the high energy demands of the new generation portable electronic devices. In this view, rechargeable Lithium-ion batteries (LIBs) are perfect candidates for energy storage requirements in various applications due to their high energy and power densities [1]. LIBs are favored over different frameworks as a result of their long cycle life, wide temperature range of operation, low self-release, no memory effect, high performance in terms of energy density and capacity [2,3]. Additionally, these batteries possess high energy conversion efficiency and zero emissions [4]. A Lithium ion battery/cell consists of a negative electrode, a positive electrode and a separator, soaked in an electrolyte solution. Every electrode is shaped from a metal substrate that is covered with a blend of an active material, an electrical conductor, a binder, and a solvent [5]. A typical anode ought to have a high Li

stockpiling limit and great basic steadiness for long cyclability and cell life. Till date, graphite is the most commonly used anode material as a part of LIB [6]. Thus, the attributes and properties of graphitic carbons have been concentrated widely [7,3,8]. It is also economical compared with other anode materials and is accessible in vast amount. The theoretical specific capacity of graphite which is 372 mAh/g. However, it is difficult to achieve this capacity in practical terms. A range of carbonaceous materials viz hard carbons, [9] single walled carbon nanotubes (SWCNT), [10,11] multiwalled carbon nanotubes (MWCNT), [12-14] graphene, [15,16] mesocarbon micro beads (MCMB) [17,18] etc., have been investigated as the anode materials for LIB. Amongst carbon nanostructures, carbon nanotubes (CNTs) have been found very important material in LIBs application. Because of their excellent electrochemical, electrical and mechanical properties these are a promising material for use in LIB [19]. The incorporation of CNTs (rather than conventional carbon) with lower weight loading is used to build up an electrical percolation system effectively. In addition, CNTs have the ability to be assembled into free-

standing anodes as an active material for lithium ion storage. Free-standing paper electrode has few points of interest, most importantly, elimination of conducting material like carbon black (to increase the conductivity of the anode) and current collector, the dead weight of an electrode is minimized, prompting the expansion of accessible limit and particular energy density of the battery [**19**] in flexible and lightweight electronic gadget applications.

Several researchers have investigated the electrochemical properties of SWCNTs, [**20-22**] MWCNTs, [**23,24**] graphene, [**25-27**] and graphene-MWCNTs hybrids [**28-30**] as an electrode for Li-ion batteries. A combination of metal/metal oxide particles on the surface of MWCNTs to increase the charge capacity is also one of the areas of recent research [**31-33**]. However, the problem of volume expansion of electrode results in the formation of defects in the electrodes after few cycles resulting in a decrease in the cell performance [**34,35**]. In one of the studies, Maurin has reported the capacity of 180 mAh/g for MWCNT based electrode [**36**]. The MWCNTs used for this purpose were synthesized by an electric-arc technique which is not only very costly but also the CNT soot was full of impurities in the form of catalyst particles, carbon onions and amorphous carbon. Yan et al. prepared different CNT based electrodes and found that a neat CNT electrode exhibits a reversible capacity of only ∼120 mAh/g during the cyclic process, a TiO_2/CNTs electrode shows reversible capacity of ∼145 mAh/g after 30 cycles and the Ag–TiO_2/CNTs electrode shows 172 mAh/g after 30 cycles [**37**]. Wang *et al.* used long length CNTs and found the reversible capacity of 290 mAh/g after 30 cycles with a Coulombic efficiency of 60% [**38**]. However, Wang et al. chose the base material as foam Ni plate, but high density of Ni which in turn accounted for the reduced energy density of the battery. Frackowiak *et al.* used MWCNTs synthesized at 900 °C which showed irreversible capacity of 505 mAh/g in second cycle, which got reduced to 273 mAh/g only after five cycles [**39**]. Pure MWCNT based paper is a good alternate over the graphite based anode materials but a sharp decline in the cell performance after few cycles as reported above could be due to disintegration of the CNT paper during charge discharge process. Keeping the above points in view, the present study was undertaken to improve the mechanical properties of the flexible anode without sacrificing its electrochemical performance. In this study, we report the fabrication of highly flexible PVDF-MWCNT composite paper with good mechanical strength and reasonably attractive electrochemical performance.

Experimental

Synthesis of carbon nanotube

Carbon nanotubes were synthesized by in-house chemical vapor deposition (CVD) setup reported earlier [**40**]. Once the temperature was reached, the arrangement containing a solution of ferrocene ($Fe(C_5H_5)_2$) (Loba), an organometallic compound, dissolved in toluene

($C_6H_5CH_3$) (SRL), in specific proportion was introduced in the reaction zone using high purity argon as a carrier gas. MWCNT were grown inside the quartz reactor, which act as a substrate itself, by thermal decomposition of hydrocarbon, in presence of iron catalyst. After the whole solution was consumed the nanotubes were harvested.

Preparation of composite paper anode

A novel route was followed for the dispersion of PVDF-MWCNT (Alpha Aesar) mix with acetone. PVDF and MWCNTs in specific proportion (10:90 ratio by weight) were mixed with acetone (SRL) by homogenizer (Miccra D-9, from ART Prozess and Labortechnik GmbH and Co. KG) then sonicated in the ultrasonicator bath to make a homogeneous mixture. In this process, the MWCNTs bundles were well de-agglomerated in the PVDF. This homogeneous mixture was transferred to specially designed vacuum filtration unit shown in the **Fig. 1**.
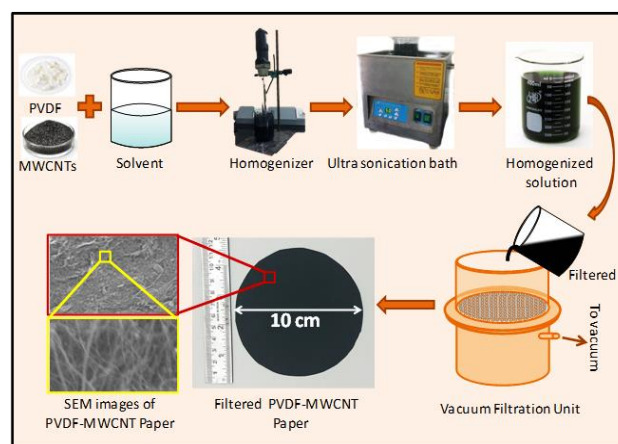

Fig. 1. Schematic of fabrication process for PVDF-MWCNT composite paper.

The composite perform paper was peeled off from the filter paper and dried between stainless steel die plates in oven at 60 ℃ to avoid formation of wrinkles due to PVDF-MWCNT interfacial interactions in the paper. MWCNT paper is also prepared by the same method without adding PVDF. The flexibility of the PVDF-MWCNT composite paper is shown in **Fig. 2**.
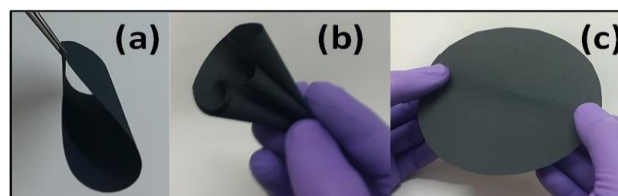

Fig. 2. Digital images of (a) single folded, (b) multiple folded and (c) unfolded PVDF-MWCNT composite paper.

Fabrication of coin cell

For making the coin cell, 18 mm diameter circular disc was cut from the composite paper sample and dried in an

oven. Free standing electrode (circular disk) was then assembled into 2032coin cell as anode in which lithium foil (Hoschen) was used as a counter electrode as shown in **Fig. 3**. Polypropylene film (Hoschen) was used as a separator and 1 M $LiPF_6$ in 1:1 proportion of ethylene carbonate and diethyl carbonate (EC + DEC) (Merk) as an organic electrolyte. The complete cell was assembled inside the argon filled glove box. The cell was allowed to stabilize for 24 h.
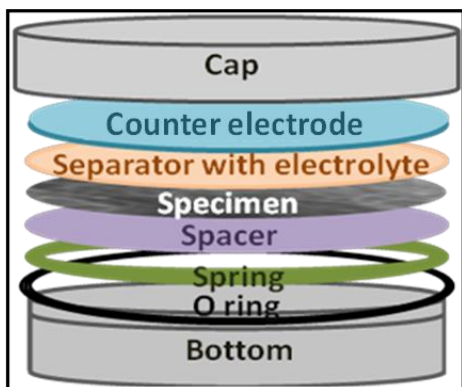

Fig. 3. Schematic of fabrication for Lithium ion coin cell.

Characterization

A Field Emission Scanning electron microscopy (FESEM) (Zeiss Supra-40VP) was used to study the morphologies of as produced MWCNTs, MWCNT paper and PVDF-MWCNT composite paper. High Resolution-Transmission Electron Microscope, Tecnai G20-string operated at 300 KV, was used for structural investigation. The Raman spectroscopy of the samples was carried out on a Renishaw inVia Raman spectrometer (UK) with laser excitation source of 514.5 nm. The tensile strength of the MWCNT and PVDF-MWCNT composite paper was measured using an INSTRON machine (model 4411). The size of the sample was 40 mm x 10 mm. The thickness of the paper was measured at several points and an average taken for the measurement of cross-sectional area. The cross-head speed was maintained at 0.2 mm/min. The surface area of the composite paper was measured by N_2 adsorption isotherm using Brunauer, Emmett and Teller (BET) method on an autosorb iQ automated gas sorption analyzer from Quantacrome Instruments, USA (model no. ASIQM0000-4). The electrical conductivity of the paper was measured by four-probe contact method using a Keithley 197 auto running advanced microvoltmeter and a Keithley 224 programmable current source. The values reported in the text are average of five readings at different places on the specimens. Galvanostatic charge/discharge characteristic of the individual coin cell was carried out at a current density of 100 mA/g. Electrochemical Impedance Studies were carried out by using an EG & G instruments Model 5210 with an AC voltage signal of 5 mV in the frequency range 100 KHz to 5 mHz. The charge–discharge cycle was carried out at C/10 rate within the voltage window of 0.01–3.0 V at room temperature.

Results and discussion

SEM, TEM and EDS

The surface morphology of the samples was studied using FESEM. **Fig. 4(a) & 4(b)** shows the scanning electron micrograph of PVDF-MWCNT composite paper at different magnification. It is observed that the MWCNTs are highly entangled with each other due to their high aspect ratio (long length). The physical interlocking of the tubes provides sufficient flexibility and handling strength to the paper to make it free standing. Inset of **Fig. 4(b)** is the cross-sectional view of the same paper showing the average thickness of the PVDF-MWCNT composite paper to be 100 µm. From the micrograph of HRTEM **(Fig. 4c)** the diameter of the MWCNTs is observed 25-50 nm. The HRTEM micrograph of the samples clearly shows webs of thin PVDF matrix supporting the CNT porous network **(Fig. 4d)** which provides greater stability to the paper. The porosity favors the ion insertion/extraction and transportation [**41**]. The presence of iron catalyst between the walls of nanotube is also observed at some places **(Fig. 4c)** [**42**].
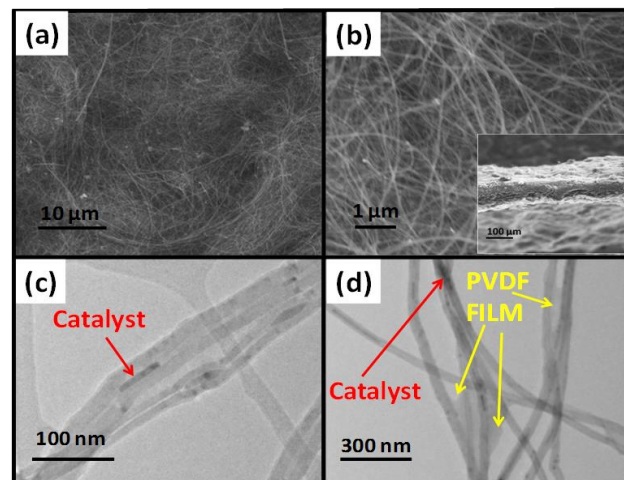

Fig. 4. (a & b) Scanning electron micrograph of PVDF-MWCNT composite paper at different magnification and (c & d) transmission electron micrograph of MWCNT paper and PVDF-MWCNT composite paper, respectively.
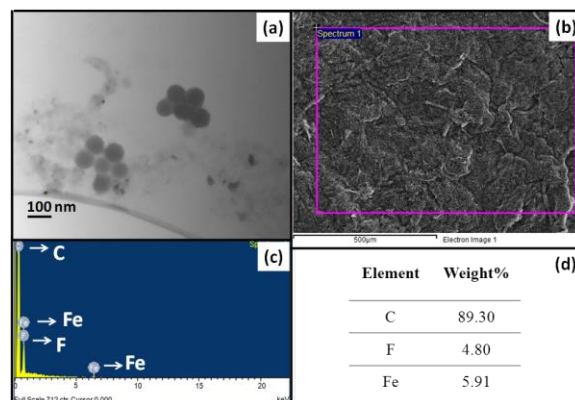

Fig. 5. (a) TEM image of PVDF powder, (b) SEM of scanned area of PVDF-MWCNT composite paper for EDS, (c) Count spectrum of composite paper and (d) Table of elements and weight percent found by EDS.

Fig. 5(a) is the TEM image of the as such PVDF powder. The shape of the granules is almost spherical and approx. 80 nm in size. **Fig. 5(b)** is a small scanned area of the composite paper which is nearly 850 µm^2. Making use of the EDS of the PVDF-MWCNT composite paper **(Fig. 5c)** shows 4.8% of Fluorine by weight in the structure which amounts to ~10% PVDF content in the composite paper which is nearly the same used initially as a binder. The iron content in the composite paper is found to be 5.91%.

XRD and Raman

The X-ray diffraction pattern using PVDF is shown in **Fig. 6(a)**. The CuKα radiation (λ= 1.54 Å) was used as X-ray source. Three prominent diffraction peaks were observed at 18.2°, 19.9°, and 26.6°, which correspond to (020), (110), (021) diffraction planes respectively of the α phase of PVDF. The PVDF usually shows three phases α, β and γ. It therefore seems that the broad diffraction maxima around 2θ = 40° is due to diffraction maxima corresponding to (201) and (111) planes of the β phase caused by the molecular head–head and tail–tail (HHTT) molecular arrangement [**43**].
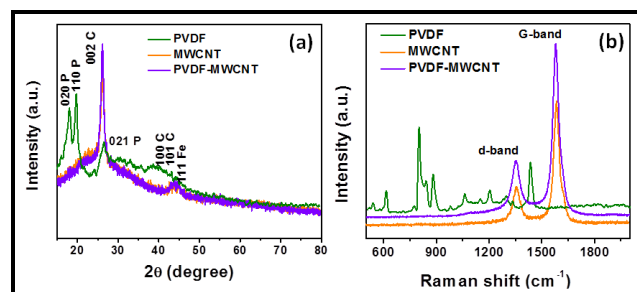
Fig. 6. (a) XRD pattern and (b) RAMAN spectra of PVDF powder, MWCNT paper and PVDF-MWCNT composite paper.

The XRD of MWCNT paper shows the prominent (002) diffraction maxima centered at 2θ=26° due to basal planes of graphite [44]. There is not much difference in the diffraction pattern from the PVDF-MWCNT composite paper due to higher intensity of reflection from carbon rather than 10% PVDF as matrix. A broad diffraction maxima hump is observed between 42.3° and 44.8° due to unresolved (100) and (101) diffraction peaks of graphite.

Fig. 6 (b) shows the Raman spectra of PVDF powder with characteristic peaks at 536 cm^{-1}, 795 cm^{-1}, 839 cm^{-1}, 882 cm^{-1}, 1296 cm^{-1} and 1428 cm^{-1} respectively [45,46]. The first order Raman spectra of the MWCNT paper shows two peaks at 1355 cm^{-1} and 1583 cm^{-1} corresponding to graphite D and G-band, respectively. However, these peaks shift to 1351 cm^{-1} (D-band) and 1578 cm^{-1} (G-band) due to the interaction between PVDF and nanotubes in the PVDF-MWCNT composite paper. The D-band is observed due to the longitudinal optical phonon induced by disordered carbon and coupled with the vibration of sp^3 bonded carbon atom related to the diamond like structures. While, the G-band arises as a

result of tangential shear mode of carbon atoms (matching to the E$_{2g}$ mode) and typically associated with the vibration of sp^2-bonded carbon atoms in a 2D hexagonal lattice, as seen in layers of graphene [**47**]. For polycrystalline graphite, it is observed that the intensity ratio D and G-band (I$_D$/I$_G$) is inversely proportional to the effective crystallite size of the graphite plane (La). The ratio is found to be nearly same i.e. 0.298 and 0.316 for MWCNT and PVDF-MWCNT for the two papers, suggesting that there is no damage to the nanotube structure due to high energy homogenizer used in the present study for dispersion.

Electrical properties and surface area

The calculated electrical conductivity of the MWCNT paper and PVDF-MWCNT composite paper is presented in **Table 1**. Electrical conductivity measurements are carried out at room temperature. Primarily, the electrical conductivity of neat MWCNT paper is found to be 30 S/cm. This high conductivity of paper is achieved due to the combine effect of high aspect ratio of MWCNT and interconnected conducting system provide by MWCNT, that results in a persistent charge distribution throughout the paper. On the other hand, in case of PVDF-MWCNT composite paper electrical conductivity decreases and is found to be 23 S/cm. This drop off is already expected due to the addition of PVDF which increases the interfacial resistance and hinder the movement of charge carriers. Thus, leads to decrease in electrical conductivity of PVDF-MWCNT composite paper. But this electrical conductivity is still high to transfer the charge easily.

Fig. 7 reveals that PVDF-MWCNT composite paper has significant potential in flexible electronics applications, such as irregularly shaped energy storage devices and other bendable displays. An experimental detailed Video of the flexible free-standing PVDF-MWCNT composite paper is provided in the supplementary information.
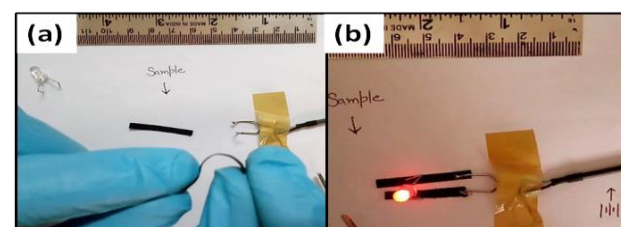

Fig. 7. (a) Digital image is showing the flexibility of PVDF-MWCNT composite paper electrode & (b) shows a red LED glowing when connected to these electrodes.

The BET surface area of the MWCNT paper and PVDF-MWCNT composite paper is found to be 63 m^2/g and 49 m^2/g, respectively **(Table 1)**. The decrease in surface area is again due to the addition of PVDF which cover up the open pores and MWCNTs surface and decreases the overall surface area of composite paper.

Table 1. Electrical properties and surface area of MWCNT paper and PVDF-MWCNT composite paper.

Sample	Conductivity (S/cm)	BET surface area (m²/g)
MWCNT paper	30	63
PVDF-MWCNT composite paper	23	49

Mechanical testing

Fig. 8, compares the stress-strain behavior of as produced MWCNT paper and PVDF-MWCNT composite paper under tensile load. It is observed that the fracture behavior of the two papers is quite different. As observed from the figure the MWCNT paper fails at a much lower load with a strain to failure of only 3.8%. The calculated value of the corresponding tensile strength is also very poor i.e. 0.26 MPa. On the other hand, the PVDF-MWCNT composite paper shows the tensile strength of 3.5 MPa and strain to failure of 11.25%.
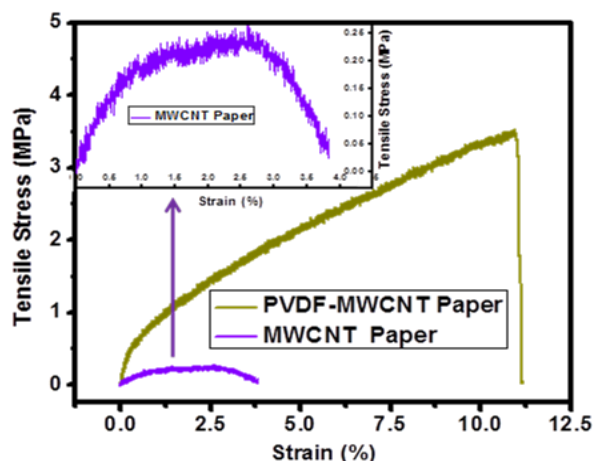
Fig. 8. Stress-Strain curves of MWCNT and PVDF-MWCNT composite Paper. Inset shows the enlarge view of the stress-strain curve of MWCNT paper.

The results show a good bonding of PVDF matrix with the porous CNT network as also revealed in the TEM micrograph of the sample in **Fig. 4**(**d**). Interestingly, a close look at the fracture surfaces of the two samples (**Fig. 9**) is quite different. In the sample without binder the crack propagates through the sample very easily leading to complete fracture of the sample at very low load. On the other hand, in the second sample the load is shared by the PVDF matrix and additional energy is consumed by the matrix to debond from the CNT leading to crack deflection.

The crack initiated from the other surface is also arrested before progressing catastrophically to the other end. The energy so absorbed in the samples therefore result into higher strength and strain to fracture of the composite sample. The high value of strain to fracture and strength along with higher flexibility will provide much needed robustness to the anode material during fabrication of battery and its longer life. Jia et. al. fabricated V_2O_5 nanowire based CNT/V_2O_5 composite

paper and measured the tensile strength value upto 4.7 MPa with strain to failure of only 2.8% [**48**]. They accredited the improvement in the mechanical performance of the composite electrode to the perforate structure of the long length PVDF coated MWCNTs [**48,49**]. However, the fabrication route in itself is quite complicated, first forming aero gel and later heating in an autoclave etc. The route adopted in the present study is much simpler comparatively.
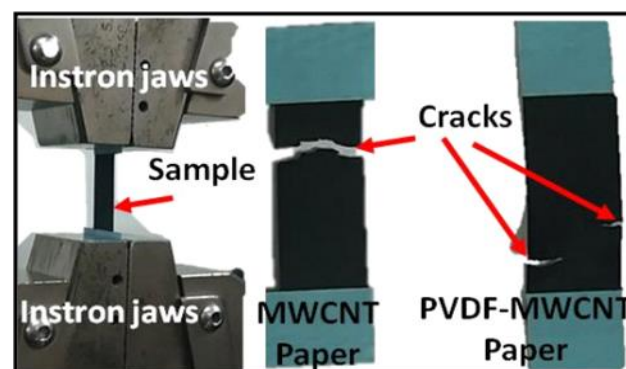

Fig. 9. Digital photographs of fractured samples of MWCNT and PVDF-MWCNT composite paper.

Electrochemical studies

Fig. 10(a) shows the galvanostatic charge/discharge characteristic of the unit coil cell after first, second and 50th cycles performed in the voltage range from 0.1 V to 3.0 V at a current density of 100 mA/g. The discharge behavior of the cell is much different in the second cycle as compared to first cycle due to the formation of solid electrolyte interface (SEI) layer on the anode [**50,51**]. As shown in the figure the charge capacity, which was 783 mAh/g in the first cycle was reduced to 217 mAh/g, after the second cycle, suggesting a Coulombic efficiency of 27% only. A close look at the first discharge cycle shows the presence of two distinct plateaus at 1.47 V and 0.79 V vs. Li⁺/Li signifying the structural transformation of the electrode due to Li insertion in the lattice. The low Coulombic efficiency for the first cycle can be ascribed to the formation of SEI layer. However, PVDF-MWCNT composite paper electrode shows indications of good electrochemical stability as well as capacity retention upto 50 cycles. This could be due to the presence of relatively high surface area and interconnected conducting network of the MWCNT which can make good contact with the electrolyte. Furthermore, researchers demonstrated that the interaction potential at the innermost region is dependent on the nanotubes diameter and MWCNTs with a diameter of 40-60 nm possesses greater interaction energy, which contribute in improving the Li storage capacity [**52,53**]. This support our study as MWCNT used in composite paper have diameter upto 50 nm and together with PVDF provide better electrochemical performance and long cycle stability with good Coulombic efficiency.

As observed in **Fig. 10(a),** the voltage profiles become quite unusual with no perceptible voltage plateaus

between these voltage ranges. However, after the initial drop the cycling performance of the cell with PVDF-MWCNT anode shows a specific capacity of 170 mAh/g even after 50 cycles as shown in figure 10(b). The Coulombic efficiency reaches almost 98% showing excellent reversibility in the charge/discharge characteristics of the cell. The value of specific capacity is significantly higher with the additional advantage of flexibility and easy processing compare to our previous report [**54**].
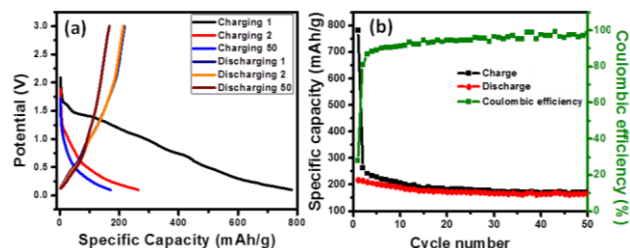

Fig. 10. (a) Electrochemical performance of the PVDF-MWCNT composite paper anodes showing 1st, 2nd and 5th cycle charge/discharge curves and (b) specific capacity and Coulombic efficiency vs. cycling number.

Electrochemical impedance spectroscopy (EIS)

For a typical lithium cell EIS provides excellent electroanalysis of the charge transfer reactions at the surface of the electrode, mass transport, double layer capacitance and the stability of the interface. In the present study, electrochemical impedance spectroscopy (EIS) of the sample was carried out by the using galvanostatic charge/discharge cycles upto fifty cycles in the frequency range of 100 kHz to 5 mHz. A common way to display the impedance of a system is with a Nyquist plot shown in **Fig. 11(a)** in which the negative imaginary component of impedance is plotted against the real component of impedance.
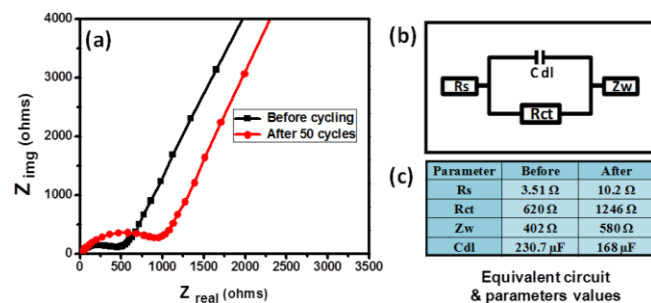
Fig. 11. (a) Nyquist plot of the PVDF-MWCNT composite paper before and after cycling, (b) the equivalent circuit and (c) table shows the parameters values of the equivalent circuit.

The Nyquist plot shows an increase in the diameter of the semicircle with the number of cycles with almost zero to 1000ohm due to combination of charge transfer resistance, capacitance and surface reactions at the electrode, forming SEI. This semi-circle is followed by a tail which is principally affected by the diffusion within the electrolyte and active electrode material [**55,56**]. The impedance spectra for PVDF-MWCNT composite paper

electrode can be modeled by an equivalent circuit in order to fit the EIS response. The equivalent circuit is provided in the **Fig. 11(b),** which is formed from the arrangement of a capacitance, resistance and constant phase element of the anode. The parameters were calculated after fitting the impedance plot and given in the Table of **Fig. 11(c)**. In equivalent circuit the R_s is the resistance due to surface film (SEI) formed on the outer surface of the electrode, R_{ct} and C_{dl} is the charge transfer resistance and the double layer capacitance, respectively, while Z_W is the Warburg impedance represents the diffusion of Li-ions in bulk of composite paper electrode. Values of all the parameters based on fitting EIS data are given in table of **Fig. 11(c)**. After analyzing the data, it can be seen clearly that R_s and R_{ct} increases after cycling while C_{dl} decreases after cycling. A possible reason for this change can be linked to the structural stability of PVDF-MWCNT composite paper. The charge transfer resistance (distance across of the half circle) increases after 50 cycles because of SEI development in initial cycles and a stable SEI layer which does not crack after cycling thus increases the resistance and decreases the capacitance value. Due to the formation of SEI layer some irreversible capacity appears. The PVDF-MWCNT structure provides a robust and stable anode. The electrode kept its structure unchanged with an interpenetrating system and shows it's mechanical robustness. Therefore, with advantages of straightforward vacuum filtration techniques for composite paper preparation and encouraging electrochemical performance, PVDF-MWCNT composite paper can be used as potential candidates as an anode material of next-generation LIB. Additionally, the free-standing composite paper electrode is prepared with reasonably reduced cost as no conductivity additive and copper current collector were used.

Conclusions

It has been possible to produce flexible, light-weight, electrically conducting and free-standing PVDF-MWCNT composite paper with tensile strength of 3.5 MPa at 11.25% strain to failure. It is therefore possible to eliminate copper substrate and increase the overall charge density of the anode. The in-house prepared large aspect ratio MWCNT were well dispersed in the solvent with the help of high energy homogenizer before processing into a flexible paper using in-house assembled vacuum filtration unit. The electrochemical performance of composite paper shows a high reversible limit of 170 mAh/g at a current density of 100 mA/g, and having Coulombic efficiency more than 98% even after fifty cycles. The flexible, light-weight and free-standing PVDF-MWCNT composite paper could be a suitable candidate as anode material for flexible or bendable next generation Li-ion batteries.
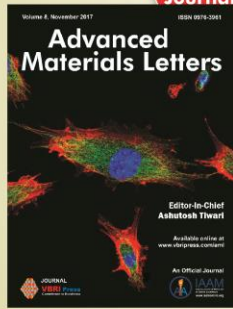
References

1. Guler, M. O.; Cetinkaya, T.; Uysal, M.; Akbulut, H.; *International Journal of Energy Research* **2015,** 39, 172.
   DOI: 10.1002/er.3220
2. Goodenough, J. B.; Kim, Y.; *Chemistry of Materials* **2010,** 22, 587.
   DOI: 10.1021/cm901452z
3. Shi, L.; Li, H.; Wang, Z.; Huang, X.; Chen, L.; *Journal of Materials Chemistry* **2001,** 11, 1502.
   DOI: 10.1039/b009907o
4. Park, M.; Zhang, X.; Chung, M.; Less, G. B.; Sastry, A. M.; *Journal of Power Sources* **2010,** 195, 7904.
   DOI: 10.1016/j.jpowsour.2010.06.060
5. Zhang, L.-S.; Jiang, L.-Y.; Yan, H.-J.; Wang, W. D.; Wang, W.; Song, W.-G.; Guo, Y.-G.; Wan, L.-J.; *Journal of Materials Chemistry* **2010,** 20, 5462.
   DOI: 10.1039/c0jm00672f
6. Xu, X.-B.; Geng, H.-Z.; Meng, Y.; Ding, E.-X.; Wang, Y.; Zhang, Z.-C.; Wang, W.-Y.; *Materials Chemistry and Physics* **2015,** 153, 155.
   DOI: 10.1016/j.matchemphys.2014.12.047
7. Lou, X. W.; Deng, D.; Lee, J. Y.; Feng, J.; Archer, L. A.; *Adv. Mater.* **2008,** 20, 258.
   DOI: 10.1002/adma.200702412
8. Li, Y.; Tan, B.; Wu, Y.; *Nano Lett.* **2008,** 8, 265.
   DOI: 10.1021/nl0725906
9. Meduri, P.; Pendyala, C.; Kumar, V.; Sumanasekera, G. U.; Sunkara, M. K.; *Nano Lett.* **2009,** 9, 612.
   DOI: 10.1021/nl802864a
10. Ban, C.; Wu, Z.; Gillaspie, D. T.; Chen, L.; Yan, Y.; Blackburn, J. L.; Dillon, A. C.; *Adv. Mater.* **2010,** 22, E145.
    DOI: 10.1002/adma.200904285
11. Ramos-Sanchez, G.; Chen, G.; Harutyunyan, A. R.; Balbuena, P. B.; *RSC Advances* **2016,** 6, 27260.
    DOI: 10.1039/c5ra27225d
12. Wang, S.; Zhang, J.; Chen, C.; *J. Power Sources* **2010,** 195, 5379.
    DOI: 10.1016/j.jpowsour.2010.03.035
13. Bulusheva, L. G.; Arkhipov, V. E.; Fedorovskaya, E. O.; Zhang, S.; Kurenya, A. G.; Kanygin, M. A.; Asanov, I. P.; Tsygankova, A. R.; Chen, X. H.; Song, H. H.; Okotrub, A. V.; *Journal of Power Sources* **2016,** 311, 42.
    DOI: 10.1016/j.jpowsour.2016.02.036
14. Pasero, D.; Reeves, N.; West, A. R.; *J. Power Sources* **2005,** 141, 156.
    DOI: 10.1016/j.jpowsour.2004.07.037
15. Noerochim, L.; Wang, J.-Z.; Chou, S.-L.; Wexler, D.; Liu, H.-K.; *Carbon* **2012,** 50, 1289.
    DOI: 10.1016/j.carbon.2011.10.049
16. Chew, S. Y.; Ng, S. H.; Wang, J.; Novák, P.; Krumeich, F.; Chou, S. L.; Chen, J.; Liu, H. K.; *Carbon* **2009,** 47, 2976.
    DOI: 10.1016/j.carbon.2009.06.045
17. Verrelli, R.; Hassoun, J.; *ChemElectroChem* **2015,** 2, 988.
    DOI:10.1002/celc.201500069
18. Landi, B. J.; Ganter, M. J.; Cress, C. D.; DiLeo, R. A.; Raffaelle, R. P.; *Energy & Environmental Science* **2009,** 2, 638.
    DOI: 10.1039/b904116h
19. Maurin, G.; Henn, F.; Simon, B.; Colomer, J. F.; Nagy, J. B.; *Nano Letters* **2001,** 1, 75.
    DOI: 10.1021/nl005517n
20. Lin, K.; Xu, Y.; He, G.; Wang, X.; *Materials Chemistry and Physics* **2006,** 99, 190.
    DOI: 10.1016/j.matchemphys.2005.09.035
21. Yang, S.; Song, H.; Chen, X.; Okotrub, A. V.; Bulusheva, L. G.; *Electrochimica Acta* **2007,** 52, 5286.
    DOI: 10.1016/j.electacta.2007.02.049
22. Ng, S. H.; Wang, J.; Guo, Z. P.; Chen, J.; Wang, G. X.; Liu, H. K.; *Electrochimica Acta* **2005,** 51, 23.
    DOI: 10.1016/j.electacta.2005.04.045
23. DiLeo, R. A.; Ganter, M. J.; Landi, B. J.; Raffaelle, R. P.; *Journal of Materials Research* **2010,** 25, 1441.
    DOI: 10.1557/JMR.2010.0184
24. Reddy, A. L. M.; Srivastava, A.; Gowda, S. R.; Gullapalli, H.; Dubey, M.; Ajayan, P. M.; *ACS Nano* **2010,** 4, 6337.
    DOI: 10.1021/nn101926g
25. Vinayan, B. P.; Nagar, R.; Raman, V.; Rajalakshmi, N.; Dhathathreyan, K. S.; Ramaprabhu, S.; *Journal of Materials Chemistry* **2012,** 22, 9949.
    DOI: 10.1039/c2jm16294f
26. Xin, F.-X.; Tian, H.-J.; Wang, X.-L.; Xu, W.; Zheng, W.-G.; Han, W.-Q.; *ACS Applied Materials & Interfaces* **2015,** 7, 7912.
    DOI: 10.1021/am508547g
27. Hu, Y.; Li, X.; Wang, J.; Li, R.; Sun, X.; *Journal of Power Sources* **2013,** 237, 41.
    DOI: 10.1016/j.jpowsour.2013.02.065
28. Lingappan, N.; Van, N. H.; Lee, S.; Kang, D. J.; *Journal of Power Sources* **2015,** 280, 39.
    DOI: 10.1016/j.jpowsour.2015.01.064
29. Yu, A.; Park, H. W.; Davies, A.; Higgins, D. C.; Chen, Z.; Xiao, X.; *The Journal of Physical Chemistry Letters* **2011,** 2, 1855.
    DOI: 10.1021/jz200836h
30. Elizabeth, I.; Mathur, R.; Maheshwari, P.; Singh, B.; Gopukumar, S.; *Electrochimica Acta* **2015,** 176, 735.
    DOI: 10.1016/j.electacta.2015.06.156
31. Stephenson, T.; Li, Z.; Olsen, B.; Mitlin, D.; *Energy & Environmental Science* **2014,** 7, 209.
    DOI: 10.1039/C3EE42591F
32. Bhaskar, A.; Deepa, M.; Narasinga Rao, T.; *ACS Applied Materials & Interfaces* **2013,** 5, 2555.
    DOI: 10.1021/am3031536
33. Zhang, W.-M.; Hu, J.-S.; Guo, Y.-G.; Zheng, S.-F.; Zhong, L.-S.; Song, W.-G.; Wan, L.-J.; *Advanced Materials* **2008,** 20, 1160.
    DOI: 10.1002/adma.200701364
34. Cui, L.-F.; Hu, L.; Choi, J. W.; Cui, Y.; *ACS Nano* **2010,** 4, 3671.
    DOI: 10.1021/nn100619m
35. Maurin, G.; Bousquet, C.; Henn, F.; Bernier, P.; Almairac, R.; Simon, B.; *Chemical Physics Letters* **1999,** 312, 14.
    DOI: 10.1016/S0009-2614(99)00886-6
36. Yan, J.; Song, H.; Yang, S.; Yan, J.; Chen, X.; *Electrochimica Acta* **2008,** 53, 6351.
    DOI: 10.1016/j.electacta.2008.04.048
37. Wang, X. X.; Wang, J. N.; Su, L. F.; *Journal of Power Sources* **2009,** 186, 194.
    DOI: 10.1016/j.jpowsour.2008.09.074
38. Frackowiak, E.; Gautier, S.; Gaucher, H.; Bonnamy, S.; Beguin, F.; *Carbon* **1999,** 37, 61.
    DOI: 10.1016/S0008-6223(98)00187-0
39. Mathur, R. B.; Chatterjee, S.; Singh, B. P.; *Composites Science and Technology* **2008,** 68, 1608.
    DOI: 10.1016/j.compscitech.2008.02.020
40. Xu, J.; Liu, Y.; He, L.; Zhang, C.; Zhang, Y.; *Ceramics International* **2016,** 42, 12027.
    DOI: 10.1016/j.ceramint.2016.04.129
41. Singh, D. K.; Iyer, P. K.; Giri, P. K.; *Diamond and Related Materials* **2010,** 19, 1281.
    DOI: 10.1016/j.diamond.2010.06.003
42. Lovinger, A. J.; Davis, D. D.; Cais, R. E.; Kometani, J. M.; *Polymer* **1987,** 28, 617.
    DOI: 10.1016/0032-3861(87)90478-2
43. Ye, M.; Hu, C.; Lv, L.; Qu, L.; *Journal of Power Sources* **2016,** 305, 106.
    DOI: 10.1016/j.jpowsour.2015.11.098
44. Satapathy, S.; Pawar, S.; Gupta, P. K.; Varma, K. B. R.; *Bulletin of Materials Science* **2011,** 34, 727.
    DOI: 10.1007/s12034-011-0187-0
45. Kobayashi, M.; Tashiro, K.; Tadokoro, H.; *Macromolecules* **1975,** 8, 158.
    DOI:10.1021/ma60044a013
46. Chaudhary, A.; Kumari, S.; Kumar, R.; Teotia, S.; Singh, B. P.; Singh, A. P.; Dhawan, S.; Dhakate, S. R.; *ACS applied materials & interfaces* **2016,** 8, 10600.
    DOI:10.1021/acsami.5b12334

47. Jia, X.; Chen, Z.; Suwarnasarn, A.; Rice, L.; Wang, X.; Sohn, H.; Zhang, Q.; Wu, B. M.; Wei, F.; Lu, Y.; *Energy & Environmental Science* **2012,** 5, 6845.
    DOI:10.1039/c2ee03110h
48. Zhang, Q.; Zhao, M.; Liu, Y.; Cao, A.; Qian, W.; Lu, Y.; Wei, F.; *Advanced Materials* **2009,** 21, 2876.
    DOI:10.1002/adma.200900123
49. Shin, H.; Park, J.; Sastry, A. M.; Lu, W.; *Journal of Power Sources* **2015,** 284, 416.
    DOI:10.1016/j.jPowsour.2015.03.039
50. Park, S. H.; Kim, H. J.; Lee, J.; Jeong, Y. K.; Choi, J. W.; Lee, H.; *ACS Applied Materials & Interfaces* **2016,** 8, 13973.
    DOI:10.1021/acsami.6b04109
51. Xiong, Z.; Yun, Y. S.; Jin, H.-J.; *Materials* **2013,** 6, 1138.
    DOI:10.3390/ma6031138
52. Zhang, Y.; Chen, T.; Wang, J.; Min, G.; Pan, L.; Song, Z.; Sun, Z.; Zhou, W.; Zhang, J.; *Applied Surface Science* **2012,** 258, 4729.
    DOI:10.1016/j.apsusc.2012.01.067
53. Teotia, S.; Singh, B. P.; Elizabeth, I.; Singh, V. N.; Ravikumar, R.; Singh, A. P.; Gopukumar, S.; Dhawan, S. K.; Srivastava, A.; Mathur, R. B.; *RSC Advances* **2014,** 4, 33168.
    DOI:10.1039/c4ra04183f
54. Ren, Y.; Wu, X.; Li, M.; *Electrochimica Acta* **2016,** 206, 328.
    DOI:10.1016/j.electacta.2016.04.161
55. Mondal, A. K.; Liu, H.; Xie, X.; Kretschmer, K.; Wang, G.; *Chem Plus Chem* **2016,** 81, 399.
    DOI:10.1002/cplu.201500528